RSC Advances

This is an *Accepted Manuscript*, which has been through the Royal Society of Chemistry peer review process and has been accepted for publication.

Accepted Manuscripts are published online shortly after acceptance, before technical editing, formatting and proof reading. Using this free service, authors can make their results available to the community, in citable form, before we publish the edited article. This *Accepted Manuscript* will be replaced by the edited, formatted and paginated article as soon as this is available.

You can find more information about *Accepted Manuscripts* in the Information for Authors.

Please note that technical editing may introduce minor changes to the text and/or graphics, which may alter content. The journal's standard Terms & Conditions and the Ethical guidelines still apply. In no event shall the Royal Society of Chemistry be held responsible for any errors or omissions in this *Accepted Manuscript* or any consequences arising from the use of any information it contains.

ROYAL SOCIETY OF CHEMISTRY

www.rsc.org/advances

Graphene foam with hierarchical structures for the removal of organic pollutants from water

Sudong Yang, Lin Chen, Lei Mu, Bin Hao, Junteng Chen, Peng-Cheng Ma*

Laboratory of Environmental Science and Technology, The Xinjiang Technical Institute of Physics and Chemistry, Key Laboratory of Functional Materials and Devices for Special Environments, Chinese Academy of Sciences, Urumqi 830011, China[1]

Abstract

Porous materials with hierarchical structures are of increasing importance because of their potential application in separation and electronic technology. Herein, three-dimensional graphene foam (GF) was prepared by using polystyrene particles as a sacrificial template and autoclaved leavening process, and the GF was further processed by carbon dioxide as an activation agent to produce meso- and nano-pores in the foam. The resulted hierarchical graphene foam (HGF) exhibits high porosity, hydrophobicity and excellent thermal stability. Compared to regular GF, due to the integration of hierarchically porous structures, HGF manifests outstanding performance for oil adsorption when applied for separating oil-water mixture, through a combination of hydrophobicity and capillary action.

[1]* Corresponding author. E-mail: mapc@ms.xjb.ac.cn. Tel.: +86-991-6992225

RSC Advances Accepted Manuscript

1. Introduction

Due to the deterioration on the oil pollution and increasing attention on the preservation of environment, there is a growing and urgent need to develop novel materials which can effectively purify the water contaminated by the petroleum products and oily compounds.[1-4] Various techniques have been proposed and employed for such cleanup, including physical adsorption, dispersant-aided diffusion, mechanical recovery by oil skimmers, in-situ burning, enhanced biodegradation, and so on.[5-7] Among the existing methods, physical adsorption by porous materials is probably the simplest and most effective technique. The principle behind this technique is that the non-polar compounds can be physically adsorbed by hydrophobic materials, and in general a high surface area and porous structure of the separators favor this process. Highly porous natural materials, such as perlite,[8] zeolite[9] and wool,[10] have been used to separate water-oil mixture. However, these materials exhibited low oil-loading capacities and poor selectivity where in most cases water and oil were adsorbed together. Therefore, much attention has been paid to develop novel materials with characters of high adsorption capacity, excellent selectivity and practical applicability for the cleanup of spilled oils and water immiscible chemicals.

Graphene-based materials were deemed as "star materials" for the removal of oily pollutants from aqueous media due to their hydrophobic and oleophilic properties. As such, fabrication of graphene into three-dimensional (3-D) materials with high surface area and controlled porosity is tremendously attractive to material scientists and greatly desirable for water-oil separation. For example, Cong et al.[11] prepared graphene-based aerogel by assembly of graphene oxide (GO) sheets and metal oxide nanoparticles, the material exhibited adsorption capacities ranging from 13 to 27 times of its own weight. Bi et al.[12] reported the use of graphene aerogels obtained from hydrothermal assembly of GO, the material exhibited adsorption capacities ranging from 20 to 86 times of its own weight, much higher than those

RSC Advances Accepted Manuscript

with natural products and polymeric foams. Besides the high adsorption of 3-D graphene, the adsorption capabilities of the materials can be easily restored by a simple thermal treatment. Zhao et al.[13] prepared nitrogen-doped graphene aerogels by hydrothermal assembly of GO in the presence of pyrrole, and the product showed improved adsorption capacity resulting from its low density.

While 3-D graphene-based frameworks, such as aerogels, foams and sponges, which exhibit continuously interconnected macro-porous structures, low mass density and large surface area, have been developed in recent years as new-generation porous carbon materials,[14-17] there are many issues to be addressed to optimize their structural, morphological and functional properties. For example, the materials generally lack well-defined meso- and/or micro-pores in the structure, which substantially limits the efficiency of adsorption for adsorbate through the capillary effect by utilizing the porous structures in the material. Therefore, construction of hierarchical architectures in 3-D graphene foams by integrating meso-porous channels within interconnected macro-porous frameworks is highly desirable.

This paper is a part of a large project in developing materials with hierarchical architectures for engineering and environmental applications. In the present paper, an autoclaved leavening process was employed to prepare graphene foam (GF) by using polystyrene (PS) particles as sacrificial template, the obtained GF was activated by carbon dioxide (CO_2) to fabricate hierarchical graphene foam (HGF). Various techniques were employed to study the morphology and surface properties of materials, and the adsorption behavior of HGF for various organic liquids and oily products was evaluated and compared with that of GF.

2. Experimental Sections

2.1 Materials

RSC Advances Accepted Manuscript

Powder-like graphite (Purity 99%, Sinopharm Chemical Reagent Co., China) was used in this study to prepare graphene. PS particles with diameter of 0.5-1.0 μm were purchased from Aladdin Reagent Co., Ltd (Shanghai, China). Hydrazine hydrate and other reagents were purchased from Beijing Chemical Reagent Factory (Beijing, China), and used as received without further purification. Deionized water was used in all experiments and generated through a Millipore Water Purification System (18.2 MΩ·cm).

2.2 Preparation of graphene foam

GF was obtained by using GO as starting material, which was synthesized from natural graphite using a modified Hummers' method.[18] In a typical experiment, GO (81 mg) was dispersed in water (40 mL) by ultrasonication for 2 h, and then mixed with PS solution with weight ratio of 9:1 under the magnetic stir for 30 min. The mixture was subjected to the vacuum filtration using a membrane filter (50 mm in diameter, 0.2 μm pore size) to get free-standing PS/GO film. The sample was processed in toluene to remove PS particles. The dried film was placed into an autoclave with the presence of hydrazine hydrate and heated to 90 °C for 12 h to obtain GF. For the activation of GF, the dried sample was heated to 800 °C in a tubular furnace for 1 h under the N_2 atmosphere. Then N_2 was switched to CO_2 to perform the activation process for 60 min to obtain HGF. For comparison, GF was prepared by the same procedure with absence of PS particles and without CO_2 activation.

2.3 Characterization

The morphology of material was observed using a scanning electron microscopy (SEM, Zeiss Supra55VP, Germany). Thermal stability of GF was characterized on a thermogravimetric analyzer (TGA, STA 449F3, Netzsch, Germany) with a heating rate of 10 °C/min from 30 to 900 °C in air condition. High resolution transmission electron microscopy (TEM) observation was carried out using a JEM-2010 (JEOL, Japan) operated at 200 kV. The surface area and pore size distribution of sample were determined by studying

RSC Advances Accepted Manuscript

the nitrogen adsorption-desorption isotherms on a surface area analyzer (Autosorb-iQ-MP, Quantachrome, USA). Surface functionalities and elemental composition of graphene materials were evaluated using an X-ray photoelectron spectroscopy (XPS, Thermo Escalab 250xi, Perkin Elmer, USA). Raman spectra were conducted on a confocal Raman spectrometer (LABRAM-HR800, Horiba Jobin-Yvon). The surface roughness of sample was measured by an atomic force microscope (AFM) under contact mode (Veeco Instruments, USA). The thermal diffusivity (α) and heat capacity (C_P) of HGF were measured using a laser flash method (LFA-447, Netzsch) at room temperature. Values on thermal conductivity (k) was calculated according to ASTM E 1461-92 standard using the equation $k = \alpha \times C_P \times \rho$, where ρ represents the density of sample. The optical images of sample were obtained by a digital camera (Canon, 600D).

2.4 Adsorption capacity of materials

The adsorption capacities of sample (Q) for various organic and oily compounds were calculated according to the following equation:

$$Q = \frac{W_{After} - W_{Before}}{W_{Before}} \quad (1)$$

Where W_{Before} and W_{After} were the weights of sample before and after immersing in a specific liquid for 20 min, respectively. The regeneration of GF with saturated-oil-adsorption was achieved by heating the sample at a temperature around the boiling point of adsorbate for 30 min, and then the dried sample was used for further cyclic operations.

3. Results and discussion

Figure 1 shows the procedure for the preparation of HGF and the morphological change of graphene-based materials at different steps. PS/GO film was easily obtained by filtering a mixture of GO and PS particles, and the film exhibited a dark brown color because of the layer-up of GO. Once the film was processed in toluene, the surface became more irregular

RSC Advances Accepted Manuscript

possibly due to the dissolution of PS and swelling effect of toluene to GO through the π-π interactions. The HGF exhibited largely convex and concave structures with large numbers of pores, suggesting the forming process of sample during the preparation and resultant increased surface roughness. It is known that GO is unstable and can be chemically reduced under mild heating to yield reduced GO and gaseous species such as H_2O and CO_2.[19,20] It was understandable that in a confined environment, the production and leakage of gases during the reduction of compact GO film by hydrazine resulted in the formation of graphene foam with porous structures. The structure was further rectified with thermal treatment under the CO_2 as carbon atoms in the graphene can be partly oxidized to form CO.

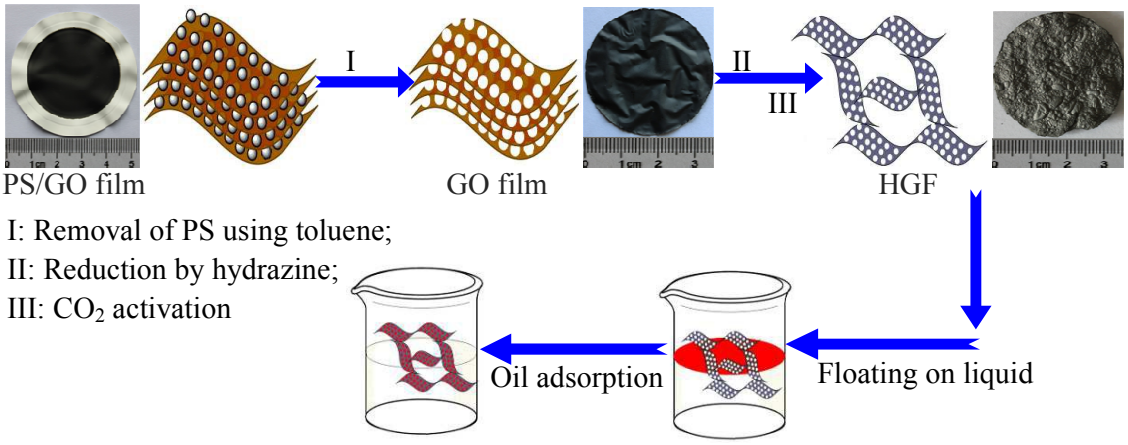

Figure 1 Schematic showing the preparation of HGF and its application for oil adsorption.

In this work, zeta potential was used to reveal the mechanism behind the interactions between the GO and PS in solution. Figure 2 shows the zeta potential of these particles in water (pH=4.5) and corresponding suspension states after 30 min of dispersion. The dispersion of PS spheres in water shows a positively charged surface with a zeta potential value of +47 mV, this high electrokinetic value makes the individual particles repel each other, resulting in an excellent suspension stability in solution. In contrast, the GO solution displays a negatively charged surface (-44 mV) due to the existence of oxygen-contained functional groups (mainly epoxide, carboxyl and hydroxyl groups). Previous report showed that an

RSC Advances Accepted Manuscript

absolute value of zeta potential at around 40 mV can be regarded as an indication of high quality dispersion for carbon-based nanoparticles,[21] confirming the outstanding suspension stability of GO in water as well.

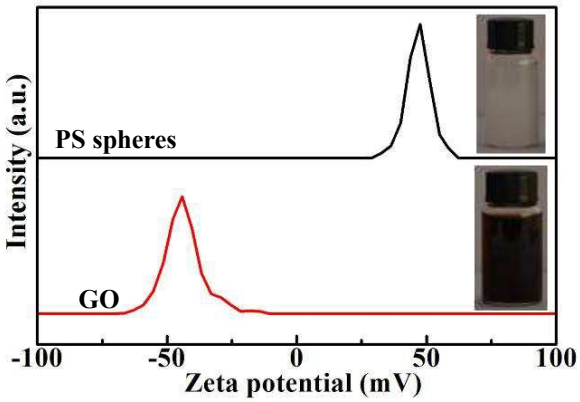

Figure 2 Zeta potential of GO and PS particles dispersed in water (pH= 4.5)

The oppositely surface charges of PS and GO particles in water led to the self-assembly of materials due to the electrostatic interactions between them,[22] which were subsequently integrated to form PS/GO film through the filtration process. This behavior brought additional benefit for the uniform distribution of PS particles in GO layers. Furthermore, the spherical PS particles on GO sheets provided spaces to effectively avoid aggregation of GO during the filtration. This assumption was partly confirmed by observing the cross-section of films using SEM, as shown in Figure 3. For PS/GO sample, the GO-wrapped PS particles were packed into multi-layers, forming crinkles and rough textures. It is noteworthy that the length of GO is much higher than the diameter of PS particles, thus results in a total wrappage for the polymer particles (Figure 3a). The PS particles in the film were selectively and easily removed by toluene, leaving behind an open porous structure without obvious collapse (Figure 3b). The excellent flexibility of GO, the controllable pore size (~0.5 μm) and weak volatility of toluene at room temperature synergistically help preserve the porous structure of GO film even after the solvent evaporation.

RSC Advances Accepted Manuscript

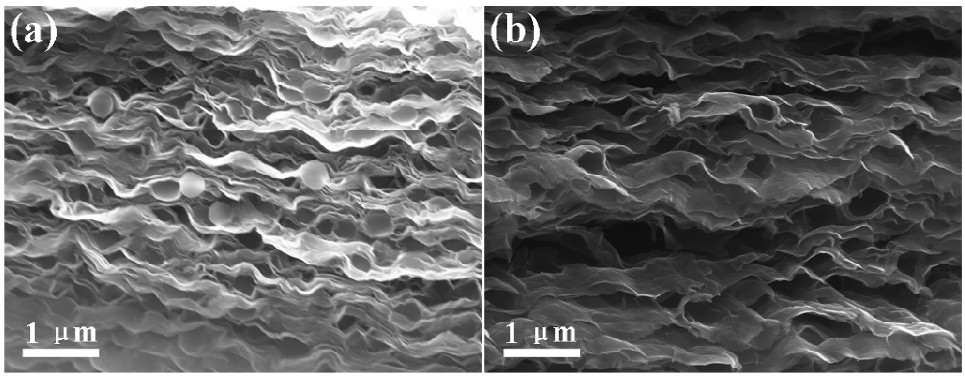

Figure 3 Cross-sectional SEM images of GO-based films (a: With PS particles; b: After removal of PS particles).

After GO film was subjected to the hydrazine treatment and following CO_2 activation, significant differences were observed on the morphology of sample. The cross-sectional SEM image (Figure 4a) shows that HGF possesses 3-D interconnected frameworks with randomly opened macro-pores with size ranging from sub-micron to up to 10 μm, and the walls in the foams are continuously linked without obvious separation between different layers. A typical SEM image with higher magnification (Figure 4b) confirms the multi-porous structures of HGF consisting of pores emanating from graphene layers with size more than 1 μm, those from PS particles with size around 0.5 μm and adjoining parts with pore size less than 0.5 μm. The top view of sample reveals that the surface of HGF exhibits numerous pores with diameter ranging from 300 to 500 nm, and adjacent pores are interconnected (c and d in Figure 4). Activation with CO_2 as gasification agent involves the oxidization of C, leading to the part burn-off of carbon atoms in graphene and consequent development of porous structure in the surface layer of HGF.[23,24] In addition, the treatment has tremendous effect on the fine structure of sample, as shown in the high-resolution TEM image of HGF (Figure 4e), numerous holes in nanometer scale are observed on the surface of graphene (as indicated by the red arrows in Figure 4e), contributing a lot for the formation of hierarchical structures of HGF with macro-, micro- and nano-scale pores.

RSC Advances Accepted Manuscript

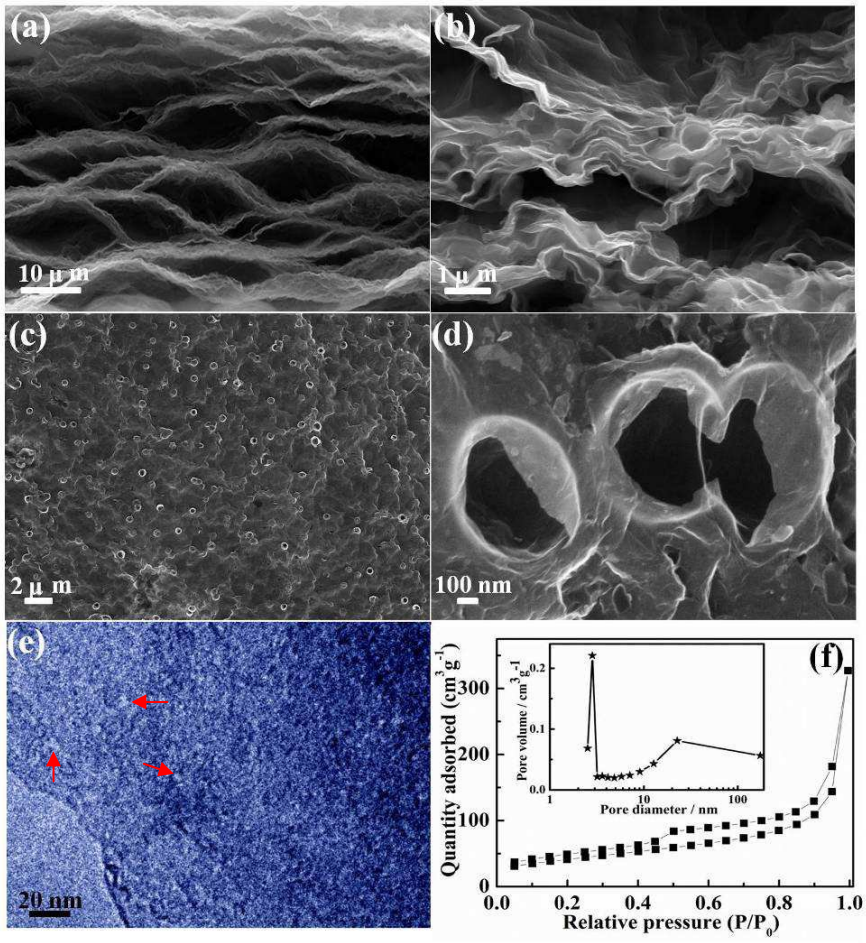

Figure 4 Morphology and pore structure of HGF (a and b: Cross-sectional SEM images; c and d: Top-view SEM images; e: Representative HRTEM image showing a meso-porous structure; f: Isotherm plot and pore distribution).

The detailed porous features of HGF were further confirmed by studying the nitrogen adsorption-desorption isotherms. As shown in Figure 4f, the curves exhibit the prominent characteristic of type-IV isotherms with a distinct hysteresis loop of H2 in the P/P_0 range of 0.4~1.0, implying the presence of relatively large macro- and meso-pores in the frameworks,[25] which is consistent with the results in Figure 4. The volume of pores calculated by the Barrett-Joyner-Halenda (BJH) method exhibits two major distributions, one locates at the pore diameter of around 2.8 nm with a peak volume of 0.23 $cm^3 \cdot g^{-1}$, and another is in the diameter of 22.6 nm with a maximum volume of 0.088 $cm^3 \cdot g^{-1}$ (inset in Figure 4f).

RSC Advances Accepted Manuscript

Brunauer-Emmett-Teller (BET) analysis reveals the sample has a specific surface area of 350 $m^2 \cdot g^{-1}$, the unique porous structure in multi-scale and high surface area of HGF endow the material a suitable candidate for various applications in adsorption and separation industry.

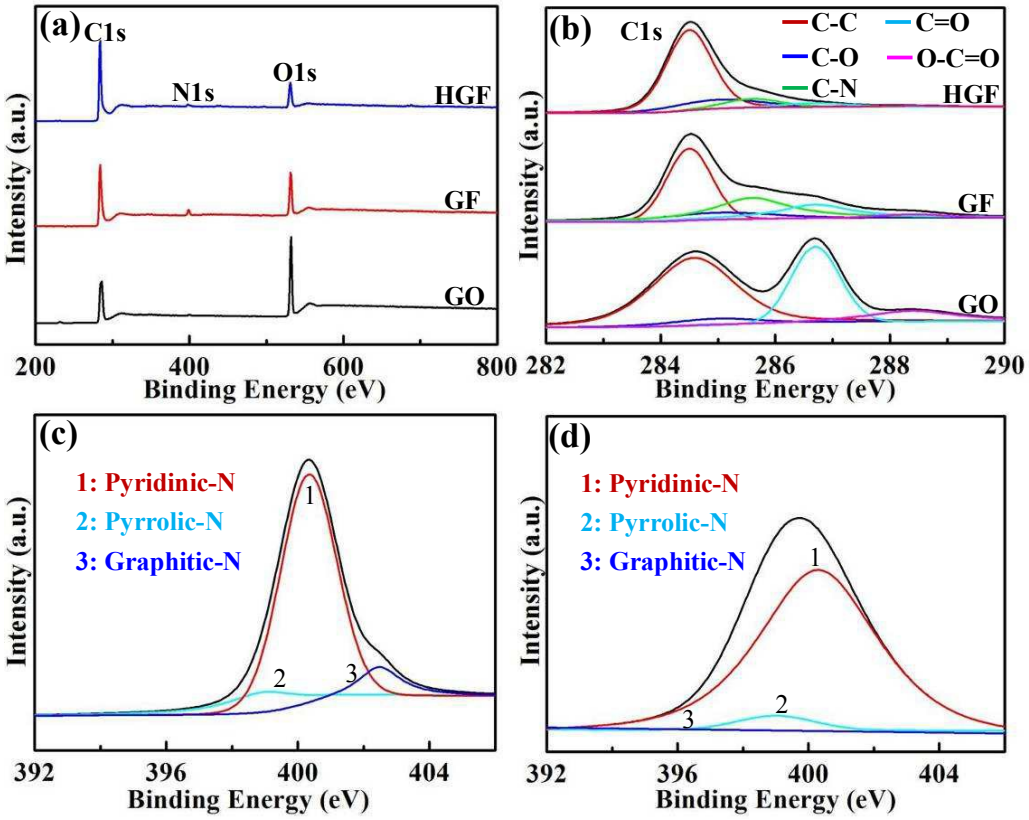

Figure 5 XPS survey spectra (a) and C1s XPS spectrum (b) of GO, GF and HGF, N1s XPS spectrum of the GF (c) and HGF (d).

Table 1 Atomic concentration of graphene-based materials.

Sample	C	O	N	O/C ratio	N/C ratio
GO	65.77	34.23	/	0.52	/
GF	75.70	19.89	4.41	0.26	0.058
HGF	85.95	11.49	2.56	0.13	0.030

XPS analysis was performed to study the chemical composition and surface information of different samples, and the results are shown in Figure 5. Only carbon and oxygen species

RSC Advances Accepted Manuscript

were detected in GO, and signals representing nitrogen were noticed in GF and HGF samples (Figure 5a). The quantitative data on the elemental composition of different samples were summarized in Table 1. The results confirmed that GO has a high concentration of oxygen. Upon hydrazine reduction, the oxygen content in the sample decreased from 34.23% to 19.89%, and HGF exhibited a lowest oxygen content among the three samples, indicating that the oxygen functionalities in GO have been removed partly. It should be noted that the nitrogen content, almost negligible in the initial GO, shows a great large amount in the reduced samples. The nitrogen atoms in the graphene most likely originated from the N_2H_4 and/or ammonia during the hydrothermal reaction. After thermal reduction, the nitrogen content decrease slightly in HGF, suggesting the recovery of aromatic structures in graphene by replacing heterogeneous atoms under the high temperature.[26]

Deconvolution on the XPS results provides information on the chemical states of elements. The deconvoluted C1s spectra for different samples are shown in Figure 5b. GO has two strong peaks at binding energies at 284.6 eV and 286.8 eV. The one with a higher binding energy corresponds to the sp^3 carbon in the form of -C-O, -C=O and O-C=O groups which resulted from the harsh oxidation and destruction of sp^2 atomic structure of graphite. The hydrazine reduction under a hydrothermal condition results in significant restoration of sp^2 carbon in the sample, as confirmed by the decreased intensities of oxygen-contained groups at binding energy at 286.8 eV. However, this process can not completely remove all oxygen functional groups, as the sample shows a decreased O/C ratio from 0.52 to 0.26, and the oxygen species are still hydroxyl, carbonyl, and carboxyl, etc. Anyway, a general tendency can be concluded that the content of hydroxyl and ether functionalities decreases.

RSC Advances Accepted Manuscript

Hydrothermal treatment to GO using N_2H_4 leads to an obvious nitrogen-doping effect in the sample. Carbon associated with nitrogen appears at binding energy of 285.3 eV, suggesting the introduction of nitrogen into GF and HGF samples. The high resolution N1s peaks of GF and HGF (c and d in Figure 5) consist of three major contributions, i.e., pyridinic-N (399.0 eV), pyrrolic-N (400.3 eV) and graphitic-N (402.5 eV).[27] After the thermal treatment, the intensity of pyridinic-N decrease significantly with a disappearance of graphitic-N, suggesting the removal of amine groups in the sample. These results confirmed further that thermal reduction is able to recover the aromatic structures by repairing defects in graphene.

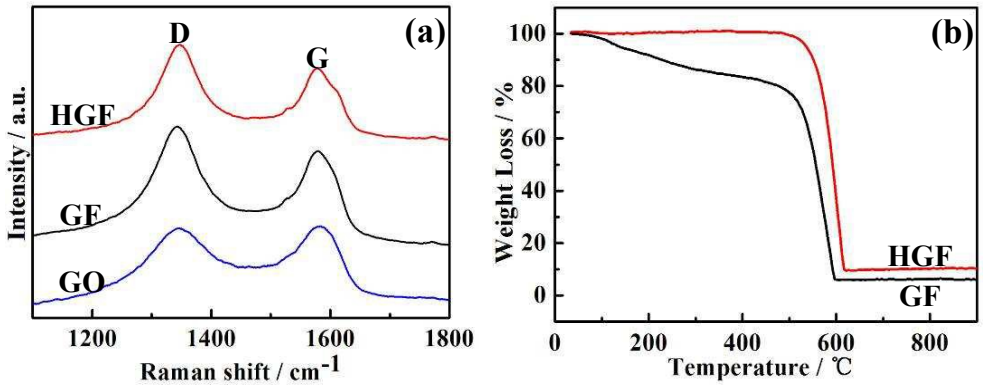

Figure 6 Raman spectra of GO, GF, and HGF (a), TGA curves of GF and HGF under air atmosphere (b).

The structural changes of different samples are reflected in their Raman spectrum. As shown in Figure 6a, the D- and G-band peak appear at about 1345 and 1581 cm^{-1}, corresponding to the disorder induced feature and the stretching vibration of C-C bond in the sample.[28] I_D/I_G (the intensity of D-band divided by that of G-band) is widely used to assess the density of defects in graphite materials. An interesting observation is that the I_D/I_G ratios show an increasing order of GO (0.95), GF (1.13) and HGF (1.21), suggesting the improvement on the disordered carbon in the sample.[29] It has been reported that upon the reduction of GO, numerous new graphitic domains were created, which exhibited a smaller

RSC Advances Accepted Manuscript

size than those present in GO before reduction,[30,31] this will decrease the average size of graphitic domains in the sample, leading to an increase in the I_D/I_G ratio.

On the other hand, the activation of GF with CO_2 significantly enhances the thermal stability of material. The TGA curves were obtained under air atmosphere with a heating rate of 10 °C min^{-1}. As shown in Figure 6b, a slight mass loss of GF occurred in the low temperature region (<200 °C), which can be ascribed to the decomposition of labile oxygen functional groups due to the chemical reduction of GO.[29] GF experiences a continuous weight loss before catastrophic failure at 500 °C. In sharp contrast, the HGF shows an excellent thermal stability without noticeable loss before 500 °C, and the carbon skeletons in the sample started to break down at 520 °C, 20 °C higher than that of GF. The rectified temperature for the combustion of HGF could be attributed to the removal of residual defects during the continuous thermal activation by CO_2 at high temperature, making the activated sample more thermally stable and enhance the inherent hydrophobic nature of HGF. Besides the excellent thermal stability, the HGF exhibits a high thermal conductivity of 26.3 W m^{-1} K^{-1}, which is more than 15 times higher than that of the foam consisting of few-layer graphene and ultrathin graphite.[32] The reason was that the interconnected architecture of HGF provided an efficient channel for the transportation of phonon, thus significantly enhance the thermal diffusion in the conduction networks.[33] The porous structure, high adsorption for organic compounds (will be discussed in the following session) and high thermal conductivity of HGF make the material a promising filler for developing 3-D polymer nanocomposites for thermal management.

To determine the average roughness, we used atomic force microscope (AFM) to measure the pure graphene foam and the modified graphene foam. Figure 7 shows the surface roughness of sample obtained from AFM. When comparing the topological differences of two samples, we observed a distinctive increase on surface roughness. HGF showed an average

RSC Advances Accepted Manuscript

mean square roughness (Ra) of 19.3 nm, much higher than that of GF (13.3 nm) within the same area scanned. Furthermore, different from GF (Figure 7a), HGF shows convex morphology in the AFM image (Figure 7b). Again, this is due to the large number of pores created on the surface of sample, which could increase the surface roughness and hierarchy of sample.

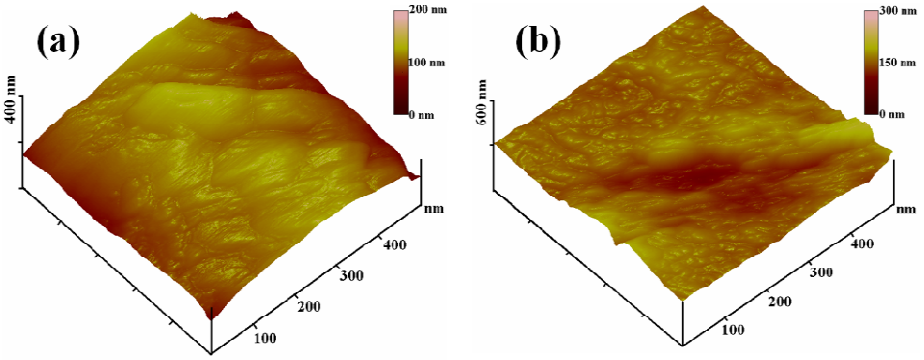

Figure 7 AFM images showing the surface roughness of samples (a: GF; b: HGF).

Wettability of material to water and oil is one of the most important considerations when selecting suitable adsorbent for the separation of oil-water mixture. Figure 8 shows the wetting behavior of HGF to water and oily droplets. The result on the measurement of contact angles shows that the sample displays a hydrophobic surface with a stable water contact angle of 106.0±1.2º (Figure 8a). When oily liquids contact with HGF, continuous spread and penetration of droplet was noticed on the sample surface (b and c in Figure 8), making it impossible to get the reliable value on contact angles. Such excellent oleophilic performance was compared by a series of consecutive photographs using two organic solvents with different viscosities, octane (0.5 cP) and oleic acid (26 cP). Quantitative data shows that the octane and oleic acid droplets can be adsorbed into the porous HGF within 0.16 s and 3.2 s, respectively. Apparently the absorption rates were associated with the viscosity of organic liquids, and a lower viscosity of adsorbate led to a faster adsorption."

RSC Advances Accepted Manuscript

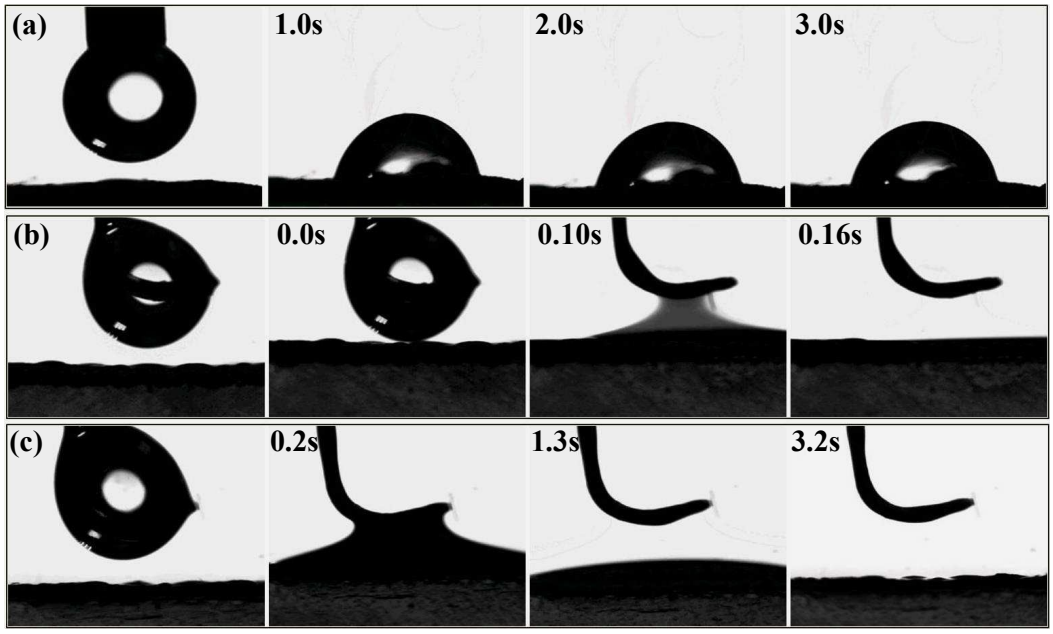

Figure 8 Wetting behavior of water (a), octane (b) and oleic acid (c) droplets on HGF surface.

The porous and interconnected framework of graphene foam provides huge space for the entrance and storage of liquids, and the hydrophobic nature of carbon make the material suitable adsorbent specifically for water-immiscible liquids. The adsorption experiment demonstrated that when a piece of HGF was placed on gasoline (dyed by Sudan I)-water mixture (Figure 9a), the foam selectively adsorbed the organic liquid from water surface and left a clear ring around the foam. The oil-filled HGF can float on water surface, which facilitated its easy collection. It usually took a few seconds to complete the adsorption, making the material a promising candidate to eliminate organic compounds in water. The adsorption capacities (Q) of two samples for various organic liquids including alkane, petroleum products and water immiscible chemicals, were tested and the results are shown in Figure 9b. The Q values of HGF for all oily liquids were over 15.0 $g \cdot g^{-1}$ and had a maximum value of 33.0 $g \cdot g^{-1}$ for olive oil. As expected, for a specific liquid, the Q value of the HGF was always higher than that of GF. The reasons for such differences are three-folds:[34-39] i) HGF

RSC Advances Accepted Manuscript

process a higher degree of pores in the structure, providing more space for the storage of adsorbed liquids. ii) The thermal annealing of HGF enhances the hydrophobicity of material to water, thus offers better affinity to the organic molecules. iii) Capillary effect is believed to be the driving force for the penetration of oil into the foams' bulk. The capillary flow is strengthened thanks to the increased olephilicity of interconnected hierarchical pores in HGF, resulting in a high adsorption capacity. In addition, the hydrophobic π-π stacking in the material and dramatically increased surface roughness may also contribute to the unusual adsorption capacities of HGF.[39] For both GF and HGF samples, the Q values for various liquids are in the same order and affected by the densities of solvents. Similar report was also found in the literature [36] and it can be explained that for a given sample, the total free volume arising from pores is a constant, results in a fixed space occupied by the oil in the sample.

The versatility of HGF was further demonstrated by measuring the oil uptake under the acidic and basic aqueous conditions. Figure 9c summarizes the adsorption capacity of HGF for three typical organic liquids (lubricate oil, octane and toluene) in different pH solutions. Marginal change was found for the performance of sample under the extreme conditions, suggesting the excellent stability of HGF against acid and alkali. The experiment for oil/water separation was carried out by using HGF as a filter. As shown in Figure 9d, the sample was fixed between the glass funnel and conical flask. When pouring the mixture consisting of heavy oil (dichloroethane dyed by Oil Red O, density=1.26 $g \cdot ml^{-1}$) and water into the facility, oil permeated through the HGF filter quickly and dropped into the conical flask. Meanwhile, water was repelled and retained on HGF surface due to the hydrophobic nature of material (Movie S1 in the Supporting Information). It should be emphasis here that the separation

RSC Advances Accepted Manuscript

process solely depends on the gravity of oil liquid without external forces, thus providing the convenience for practical application. Results after an extensive trial and error showed that such filtration process was not suitable to separate the emulsified oil/water mixture, possibly due to the small size and high stability of oil droplets in water.

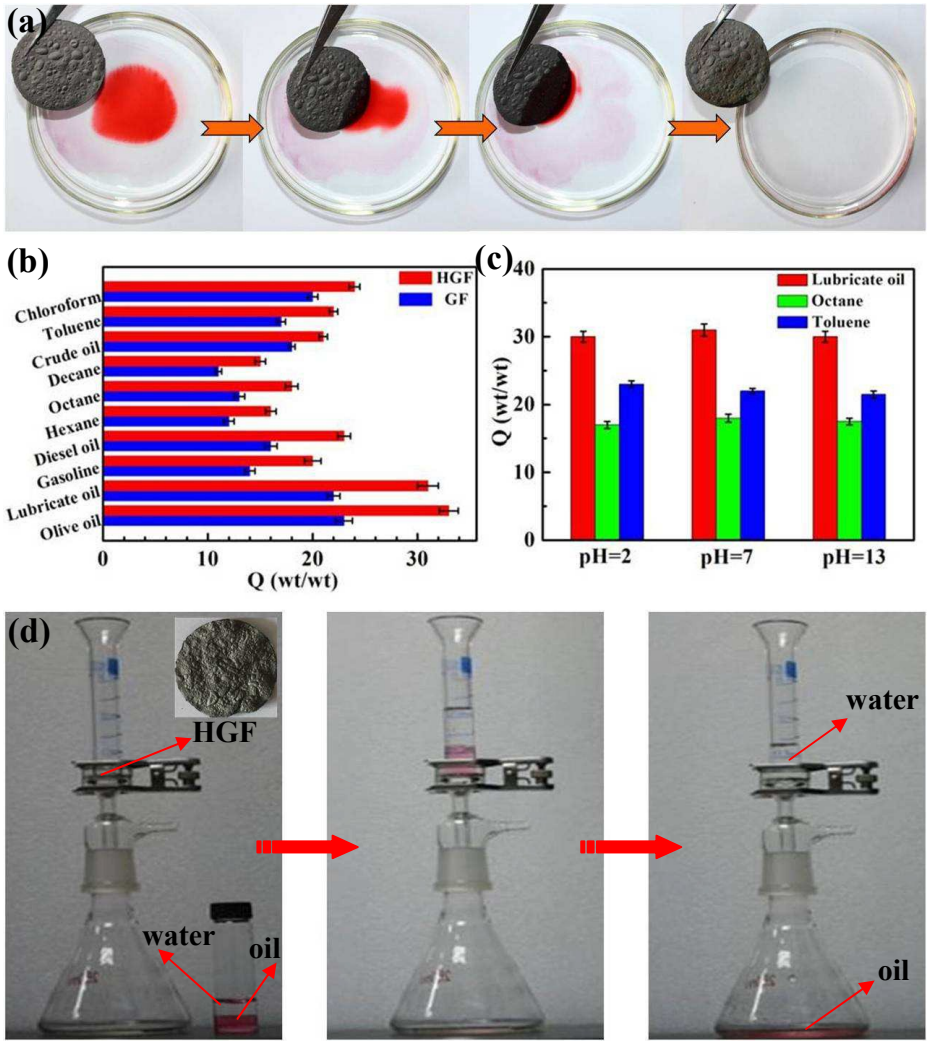

Figure 9 Oil adsorption performance of different foams (a: Illustration showing the adsorption process of HGF for gasoline; b: Adsorption capacity of GF and HGF for various organic liquids; c: Adsorption capacity of HGF for organic liquids in different aqueous solutions; d: Oil/water separation studies of the HGF. For clarity, the probe liquid, 1,2-dichloroethane was dyed by Oil Red O).

RSC Advances Accepted Manuscript

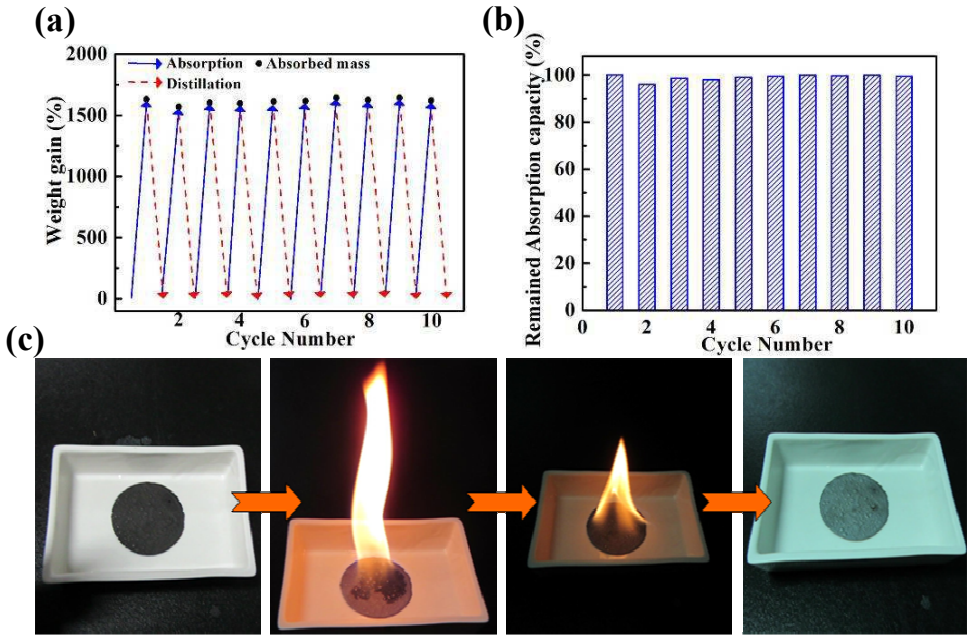

Figure 10 Recyclability and regeneration of HCF for oil adsorption (a: Adsorption recyclability of HGF over ten cycles; b: Adsorption capacity of HGF recycled via distillation; c: Photographs showing the regeneration of HCF via combustion).

Recyclability of material is a key requirement for high performance adsorbent in practical applications. These factors were evaluated through a simple adsorption-drying cycle by taking n-hexane as an example, and adsorbent was recovered by heating the sample at 70 ^{o}C (boiling point of n-hexane). HGF shows a stable adsorption capacity of 15 times of its own weight after cyclic adsorption/distillation operations (Figure 10a), and retained more than 99% of its original adsorption capacity for hexane after 10 runs (Figure 10b). Moreover, it is worth noting that the adsorbed oil and other organic solvents can be easily removed by burning (Figure 10c). Interestingly, the foam remains as an entire framework without collapse when burned in air. Furthermore, it was found that the foam had an excellent regeneration capacity, an important index of a promising adsorbent. This capability was attributed to the excellent thermal stability and fire resistance of foam, and the porous structure of material facilitated the transfer of heat generated during the combustion.

4. Conclusions

RSC Advances Accepted Manuscript

In summary, we have developed a simple method to prepare graphene foam processes macro and meso-porous structures with hierarchical features. The hierarchical graphene foam showed high porosity, excellent thermal stability, high hydrophobicity and oleophilicity, and can be employed as an efficient adsorbent for oil adsorption with favorable adsorption capacity, outstanding recyclability and high selectivity. The ease of fabrication and enhanced performance make hierarchical graphene foam as general and effective support for designing high performance environmental remediation materials, and we believe the hierarchical structure in graphene foam developed in this study may be suitable for other novel applications like 3-D electrode material in energy storage and conversion devices.

Acknowledgements

This project was supported by the Western Light (Project No. XBBS201215), the National Natural Science Foundation of China (Project Nos. 51302308, 11472294), Science and Technology Plan of Urumqi (Project No. P141010006), as well as the Research Fund for Distinguished Young Scientist in Xinjiang (Project No. 2013711005). Yang and Ma acknowledged the support from the Xinjiang High-level Talents Recruitment Plan.

Supporting Information.

Movie S1: The movie shows that oil/water separation studies using HGF.

References

1 J. K. Yuan, X. G. Liu, O. Akbulut, J. Q. Hu, S. L. Suib, J. Kong and F. Stellacci, *Nat. Nanotechnol*., 2008, **3**, 332-336.

2 M. A. Shannon, P. W. Bohn, M. Elimelech, J. G. Georgiadis, B. J. Marinas and A. M. Mayes, *Nature*, 2008, **452**, 301-310.

3 K. Li, J. Ju, Z. X. Xue, J. Ma, L. Feng, S. Gao and L. Jiang, *Nat. Commun*., 2013, **4**, 2276.

RSC Advances Accepted Manuscript

4 L. B. Zhang, Z. H. Zhang and P. Wang, *NPG Asia Mater*., 2012, **4**, e8.

5 S. D. Yang, L. Chen, L. Mu, B. Hao and P. C. Ma, *RSC Adv*., 2015, **5**, 38470-38478.

6 J. Aurell and B. K. Gullett, *Environ. Sci. Technol*., 2010, **44**, 9431-9437.

7 J. Zhao, C. F. Xiao and N. K. Xu, *J. Dispersion Sci. Technol*., 2012, **33**, 1197-1203.

8 D. Bastani, A. A. Safekordi, A. Alihosseini and V. Taghikhani, *Sep. Purif. Technol*., 2006, **52**, 295-300.

9 M. M. Radetic, D. M. Jocic, P. M. Jovanccic, Z. L. Petrovic and H. F. Thomas, *Environ. Sci. Technol*., 2003, **37**, 1008-1012.

10 A. Bayat, S. F. Aghamiri, A. Moheb and G. R. Vakili-Nezhaad, *Chem. Eng. Technol*., 2005, **28**, 1525-1528.

11 H. P. Cong, X. C. Ren, P. Wang and S. H. Yu, *ACS Nano*, 2012, **6**, 2693-2703.

12 H. C. Bi, X. Xie, K. B. Yin, Y. L. Zhou, S. Wan, L. B. He, F. Xu, F. Banhart, L. T. Sun and R. S. Ruoff, *Adv. Funct. Mater*., 2012, **22**, 4421-4425.

13 Y. Zhao, C. G. Hu, Y. Hu, H. H. Cheng, G. Q. Shi and L. T. Qu, *Angew. Chem., Int. Ed*., 2012, **51**, 11371-11375.

14 S. Nardecchia, D. Carriazo, M. L. Ferrer, M. C. Gutierrez and F. del Monte, *Chem. Soc. Rev*., 2012, **42**, 794-830.

15 H. C. Bi, X. Xie, K. B. Yin, Y. L. Zhou, S. Wan, R. S. Ruoff and L.T. Sun, *J. Mater. Chem. A*, 2014, **2**, 1652-1656.

16 Z. Q. Niu, L. L. Liu, L. Zhang and X. D. Chen, *Small*, 2014, **10**, 3434-3441.

17 J. H. Li, J. Y. Li, H. Meng, S. Y. Xie, B. W. Zhang, L. F. Li, H. J. Ma, J. Y. Zhang and M. Yu, *J. Mater. Chem. A*, 2014, **2**, 2934-2941.

RSC Advances Accepted Manuscript

18 S. D. Yang, C. M. Shen, Y. Y. Liang, H. Tong, W. He, X. Z. Shi, X. G. Zhang and H. J. Gao, *Nanoscale*, 2011, **3**, 3277-3284.

19 D. R. Dreyer, S. Park, C. W. Bielawski and R. S. Ruoff, *Chem. Soc. Rev.*, 2010, **39**, 228-240.

20 Z. Q. Niu, J. Chen, H. H. Hng, J. Ma and X. D. Chen, *Adv. Mater.*, 2012, **24**, 4144-4150.

21 P. C. Ma, N. A. Siddiqui, E. Mäder and J. K. Kim, *Compos. Sci. Technol.*, 2011, **71**, 1644-1651.

22 B. G. Choi, M. Yang, W. H. Hong, J. W. Choi and Y. S. Huh, *ACS Nano*, 2012, **6**, 4020-4028.

23 M. Turmuzi, W. R. W. Daud, S. M. Tasirin, M. S. Takriff and S. E. Iyuke, *Carbon*, 2004, **42**, 453-455.

24 W. C. Peng, S. Z. Liu, H. Q. Sun, Y. J. Yao, L. J. Zhi and S. B. Wang, *J. Mater. Chem. A*, 2013, **1**, 5854-5859.

25 Y. Tao, D. B. Kong, C. Zhang, W. Lv, M. X. Wang, B. H. Li, Z. H. Huang, F. Y. Kang and Q. H. Yang, *Carbon*, 2014, **69**, 169-177.

26 D. H. Long, W. Li, L. C. Ling, J. Miyawaki and I. Mocida, *Langmuir*, 2010, 26, 16096-16102.

27 H. Wang, T. Maiyalagna and X. Wang, *ACS Catalysis*, 2012, **2**, 781-794.

28 M. S. Dresselhaus, A. Jorio, M. Hofmann, G. Dresselhaus and R. Saito, *Nano lett.*, 2010, **10**, 751-758.

29 X. B. Li, S. W. Yang, J. Sun, P. He, X.G. Xu and G.Q. Ding, *Carbon*, 2014, **78**, 38-48.

30 S. Stankovich, D. A. Dikin, R. D. Piner, K. A. Kohlhaas, A. Kleinhammes, Y. Jia, Y. Wu, S. T. Nguyen and R. S. Ruoff, *Carbon*, 2007, **45**, 1558-1565.

RSC Advances Accepted Manuscript

31 L. G. Cançado, K. Takai, T. Enoki, M. Endo, Y. A. Kim, H. Mizusaki, A. Jorio, L. N. Coelho, R. Magalhães-Paniago and M. A. Pimenta, *Appl. Phys. Lett*., 2006, **88**, 163106.

32 M. T. Pettes, H. Ji, R. S. Ruoff and L. Shi, *Nano Lett*., 2012, **12**, 2959-2964.

33 Y. H. Zhao, Z. K. Wu and S. L. Bai, *Compos. Part A*, 2015, **72**, 200-206.

34 H. D. Liu, Z. Y. Liu, M. B. Yang and Q. He, *J. Appl. Polym. Sci*., 2013, **130**, 3530-3536.

35 S. J. Choi, T. H. Kwon, H. Im, D. I. Moon, D. J. Baek, M. L. Seol, J. P. Duarte and Y. K. Choi, *ACS Appl. Mater. Interfaces*, 2011, **3**, 4552-4556.

36 H. W. Liang, Q. F. Guan, L. F. Chen, Z. Zhu, W. J. Zhang and S. H. Yu, *Angew. Chem., Int. Ed*., 2012, **51**, 5101-5105.

37 Q. Zhu, Y. Chu, Z. K. Wang, N. Chen, L. Lin, F. T. Liu and Q. M. Pan, *J. Mater. Chem. A*, 2013, **1**, 5386-5393.

38 P. Calcagnile, D. Fragouli, I. S. Bayer, G. C. Anyfantis, L. Martiradonna, P. D. Cozzoli, R. Cingolani and A. Athanassiou, *ACS Nano*, 2012, **6**, 5413-5419.

39 J. Shieh, F. J. Hou, Y. C. Chen, H. M. Chen, S. P. Yang, C. C. Cheng and H. L. Chen, *Adv. Mater*., 2010, **22**, 597-601.

RSC Advances Accepted Manuscript

List of Captions for Tables:

Table 1 Atomic concentration of graphene-based materials.

List of Captions for Figures:

Figure 1 Schematic showing the preparation of HGF and its application for oil adsorption.

Figure 2 Zeta potential of GO and PS particles dispersed in water (pH= 4.5)

Figure 3 Cross-sectional SEM images of GO-based films (a: With PS particles; b: After removal of PS particles).

Figure 4 Morphology and pore structure of HGF (a and b: Cross-sectional SEM images; c and d: Top-view SEM images; e: Representative HRTEM image showing a meso-porous structure; f: Isotherm plot and pore distribution).

Figure 5 XPS survey spectra (a) and C1s XPS spectrum (b) of GO, GF and HGF, N1s XPS spectrum of the GF (c) and HGF (d).

Figure 6 Raman spectra of GO, GF, and HGF (a), TGA curves of GF and HGF under air atmosphere (b).

Figure 7 AFM images showing the surface roughness of samples (a: GF; b: HGF).

Figure 8 Wetting behavior of water (a), octane (b) and oleic acid (c) droplets on HGF surface.

Figure 9 Oil adsorption performance of different foams (a: Illustration showing the adsorption process of HGF for gasoline; b: Adsorption capacity of GF and HGF for various organic liquids; c: Adsorption capacity of HGF for organic liquids in different aqueous solutions; d: Oil/water separation studies of the HGF. For clarity, the probe liquid, 1,2-dichloroethane was dyed by Oil Red O.).

Figure 10 Recyclability and regeneration of HCF for oil adsorption (a: Adsorption

RSC Advances Accepted Manuscript

recyclability of HGF over ten cycles; b: Adsorption capacity of HGF recycled via distillation; c: Photographs showing the regeneration of HCF via combustion).

RSC Advances Accepted Manuscript

Graphical abstract

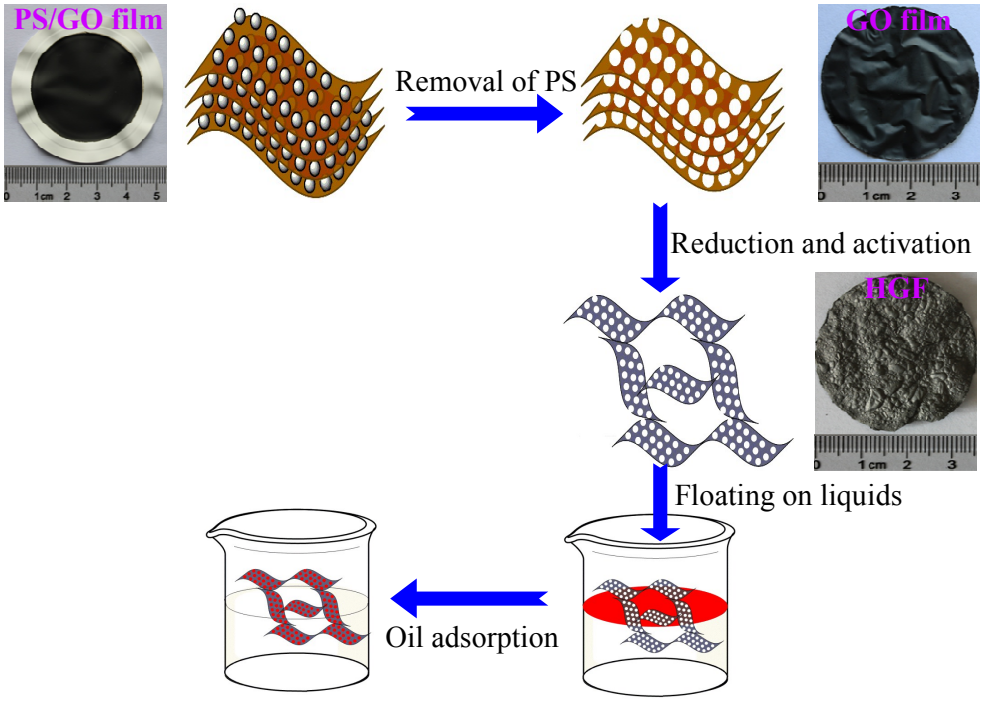

RSC Advances Accepted Manuscript